Applied Physics A (2025) 131:781
https://doi.org/10.1007/s00339-025-08895-z

Applied Physics A
Materials Science & Processing

Chemical vapor deposition of indium precursors for solar micro-absorbers using continuous laser radiation

Heike Voss[1] · Setareh Zahedi-Azad[2] · Owen C. Ernst[2,3] · Jan Lucaßen[4] · Guido Mann[5] · Jörn Bonse[1] · Torsten Boeck[2] · Jens Martin[2] · Martina Schmid[4] · Jörg Krüger[1]

Received: 17 June 2025 / Accepted: 18 August 2025 / Published online: 16 September 2025

Abstract
Localized deposition of indium on an amorphous glass surface covered with a thin molybdenum layer is demonstrated utilizing laser-assisted chemical vapor deposition. A continuous-wave laser causes a temperature rise on the molybdenum layer resulting in the selective aggregation of liquid and ultimately crystalline structures of indium. The formation sites of the indium are determined by the decomposition of gaseous trimethylindium. The deposited indium islands can serve as precursors and could be further processed into compound semiconductors like $CuInSe_2$ for micro-concentrator solar cells. The experimental investigations were supported by theoretical simulations of the laser heating process to calculate the local temperature distribution on the surface of the molybdenum-covered glass substrate.

Keywords Laser-assisted Chemical Vapor Deposition · CW Laser · Indium Islands · Micro-concentrator Solar Cell

1 Introduction

Micro-concentrator solar cells have garnered significant attention not only for their potential to enhance power conversion efficiency but also for their ability to reduce material consumption. Improved efficiency remains a central goal in photovoltaic research, and micro-concentrator devices offer a promising pathway by enabling operation beyond the Shockley-Queisser limit through optical concentration [1]. Compared to large-area solar cells, these miniaturized devices also benefit from improved thermal management and a more compact architecture. Additionally, reducing material usage is especially critical for thin-film technologies that rely on expensive or scarce elements, such as indium and gallium in $Cu(In,Ga)Se_2$ (CIGSe) solar cells [2–5].

To achieve true material savings, the CIGSe micro-absorbers must be fabricated using bottom-up processes. Subsequent fabrication of micro solar cells includes the isolation of the micro-absorbers (if not already given through the local growth process) and the deposition of front buffer and contact layers. Generally, many micro-absorbers are connected in parallel for ease of fabrication and to achieve higher currents. Arrays of micro solar cells are then to be combined with concentrator lenses for operation under enhanced irradiance and collection of all incident light despite incomplete coverage of the substrate.

A key method for bottom-up fabrication of CIGSe absorbers relies on the localized electrodeposition of metallic precursors, followed by a thermal selenization step. Selectivity in deposition stems from micro-patterned back contacts: either the molybdenum (Mo) back contact is pre-structured into micro-sized features [6], or a planar Mo back contact is locally masked by patterning SiO_2 isolation layers on top allowing only selected areas [7] to be exposed. In both cases, absorber growth occurs exclusively on the exposed Mo regions.

✉ Heike Voss
heike.voss@bam.de

[1] Bundesanstalt für Materialforschung und -prüfung (BAM), Unter den Eichen 87, 12205 Berlin, Germany

[2] Leibniz-Institut für Kristallzüchtung (IKZ), Max-Born-Str. 2, 12489 Berlin, Germany

[3] Brandenburg University of Technology Cottbus-Senftenberg (BTU), Universitätsplatz 1, 01968 Senftenberg, Germany

[4] Fakultät für Physik und CENIDE (UDE), Universität Duisburg-Essen, Forsthausweg 2, 47057 Duisburg, Germany

[5] BeamXpert GmbH, Max-Planck-Str. 3, 12489 Berlin, Germany

In addition, two laser-based, material-saving bottom-up processes to produce CISe and CIGSe absorbers were investigated in the past. The first method is based on the growth of metallic precursors on laser-structured substrates by means of physical vapor deposition (nucleation approach) [8]. The growth is driven by material collection from a surrounding catchment area, typically several hundred micrometers in radius, concentrating material transport toward laser-modified nucleation sites. The reduced adatom concentration in these surrounding areas inhibits secondary nucleation, allowing controlled formation of isolated indium islands. After copper evaporation, a thermal selenization step yields $CuInSe_2$ islands, that can serve as building blocks for micro solar cell arrays [9].

In the second laser-based method, precursors are transferred to the substrate using a femtosecond laser (laser-induced forward transfer, LIFT) [10]. Laser radiation is utilized to deposit parts of a donor film, which was previously placed on a transparent carrier medium, to a target substrate in a site-selective manner. Subsequent steps mirror those of the nucleation-based process, ultimately yielding micro-absorber islands for solar cells [11]. As a proof of concept, it was demonstrated that both, the nucleation, and the LIFT approach can in principle be used to produce precursors for solar micro-absorbers. Both methods using ultrashort laser pulses in the femtosecond regime were described in an overview article [12].

The laser techniques described above utilizing ultrashort laser pulses can be differentiated from laser processing based solely on thermal effects, such as laser annealing and chemical vapor deposition (CVD) realizing laser-heated surfaces. CVD was demonstrated using longer laser pulses in the nanosecond range [13] or even continuous-wave (cw) laser irradiation [14].

In this work, investigations of the site-controlled local growth of indium islands on molybdenum-coated glass substrates based on cw laser irradiation are performed. The aim is to achieve localized aggregation of indium on molybdenum by the pyrolytic decomposition of gaseous trimethylindium. Laser heating takes place at the localized spots onto which the laser is focused, being sufficient to decompose the precursor gas and deposit indium. A general scheme of the proposed laser-assisted metal–organic chemical vapor deposition process (LA-MOCVD) is shown in Fig. 1. Thermo-physical simulations of the laser irradiation process were carried out to analyze the necessary laser specifications and geometric parameters to produce a locally confined temperature gradient strong enough to enable the deposition of discrete indium islands. The formation of CISe micro-absorbers based on these indium islands is also demonstrated. This approach does not use complex masking or lithography processes.

2 Experimental

2.1 LA-MOCVD-cluster system

The LA-MOCVD system used at IKZ (Leibniz-Institut für Kristallzüchtung, Berlin, Germany) was custom-designed and installed by BESTEC GmbH, Berlin, Germany. It enables all the necessary steps for processing CIGSe absorbers in a batch process without breaking the vacuum by connecting three vacuum chambers through a common handling system.

The experimental setup of the LA-MOCVD chamber is sketched in Fig. 1a. Commercial $50 \times 50 \times 2$ mm^3 soda-lime floatglass samples (Weidner Glas) served as substrates. Mo layers with a thickness ranging from 275 to 800 nm were

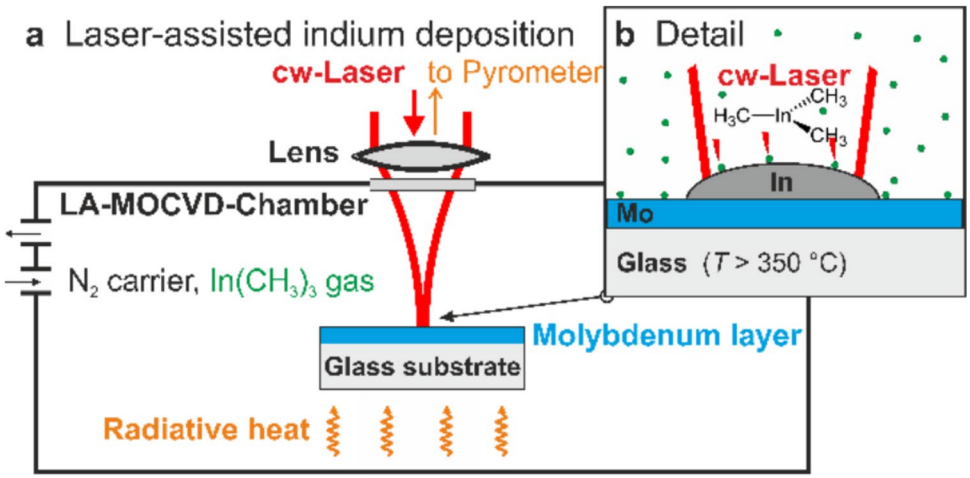

Fig. 1 **a** Sketch of the experimental setup for laser-assisted deposition of indium on molybdenum-coated glass substrates inside a LA-MOCVD chamber by localized heating with an externally mounted cw laser source focused by a lens. **b** Detail illustrating the LA-MOCVD process for laser-induced cracking of trimethylindium leading to the nucleation of indium on the surface

deposited on the substrate by electron-beam-PVD in order to create a metallic surface. The Mo deposition was conducted with a deposition rate of 1.5 Å/s at room temperature under high vacuum conditions. The resulting Mo layer exhibited a typical rms surface roughness of 1 nm.

The substrates were mounted inside the LA-MOCVD chamber which was continuously pumped to achieve a stable pressure of typically 20 mbar. Metallic precursor trimethylindium ($In(CH_3)_3$) was transferred to the gas phase in a bubbler and added to nitrogen serving as a carrier gas. This gas mixture was injected into the LA-MOCVD chamber through heated pipes (50 °C) at a flow rate of 100 sccm (standard cubic centimeters per minute) for trimethylindium and 1000 sccm for nitrogen. In the following, absolute temperatures are given in °C, while temperature differences are provided in K.

The coated glass substrate was radiatively heated to a temperature close to the temperature threshold for decomposition of trimethylindium (340 °C for nitrogen carrier gas [15]) and kept at this constant temperature during the deposition process. The temperature range was determined experimentally and set to 350 °C—380 °C.

The molybdenum film on the glass substrate inside the LA-MOCVD chamber was additionally locally heated by laser radiation of an external infrared cw laser, focused through a lens outside a window of the LA-MOCVD chamber system. Consequently, the cracking temperature of the trimethylindium gas was exceeded locally at the laser-heated metal film surface, and while being exposed to the trimethylindium gas flow the local deposition of indium on the molybdenum film was enabled (Fig. 1b).

Indium islands were successfully formed in the LA-MOCVD chamber by this laser-induced deposition. These precursor-islands were processed into $CuInSe_2$ absorbers by first depositing 800 nm of copper using e-beam technology. Subsequently, they were thermally annealed and selenized in a three-step post-process: 1) heating and melting for 10 min at 350 °C, 2) selenizing for 6 min at 700 °C, 3) annealing for 5 min at 350 °C.

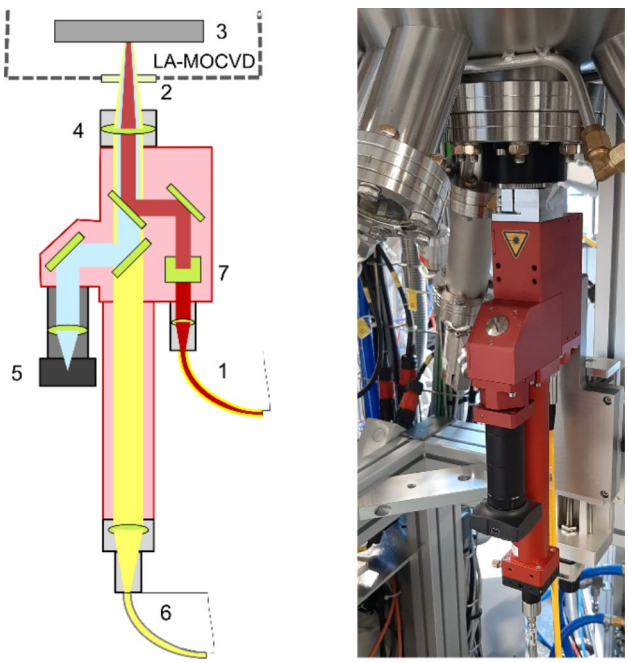

Fig. 2 Sketch (left) and photograph (right) of the laser processing head, mounted underneath the LA-MOCVD chamber on *X*-*Y*-*Z* stages, allowing for the positioning and focusing of the laser spot on the substrate inside the chamber. (1) laser fiber, (2) window, (3) sample, (4) focusing lens, (5) CCD camera, (6) pyrometer fiber, (7) attenuator

2.2 Laser setup

A laser system from Dr. Mergenthaler GmbH & Co. KG, Neu-Ulm, Germany, consisting of an ytterbium single mode fiber laser with 1070 nm wavelength and 10 W continuous power was used to locally heat the substrate. The laser radiation was delivered to a laser processing head via an optical fiber (1), as sketched in Fig. 2 (left). Here, three optical paths were combined via beam splitters to be coaxial and focused through a chamber window (2) onto the substrate (3) surface with a common lens (4) of 250 mm focal length to a Gaussian laser spot size radius of (43.5 ± 5) µm ($1/e^2$-decay) or (61.5 ± 7) µm, depending on the position of the sample surface in respect to the focal plane. Reflection of the laser radiation at the uncoated chamber window was accounted for by a reflection loss of 7%. The head was also equipped with a CCD camera (5) and an optical fiber (6) that coupled into a pyrometer to enable local relative temperature measurements at the laser-irradiated site. A polarization prism-based attenuator (7) was integrated to reduce the maximal laser power to 800 mW. Throughout this publication, laser powers are given as emitted by the laser head including the attenuation, while intensities relate to the power incident on the sample and therefore take the transfer losses at the window into account.

The attached pyrometer captured the heat radiation emitted by the substrate in a wavelength band of 2.0 µm to 2.6 µm, integrating over a spot diameter of ~ 120 µm, co-adjusted with the sample-heating laser beam. An emissivity of 0.1 for the highly reflective molybdenum layer was assumed for the calibration of the pyrometer. The pyrometer signal was recorded for each laser process and proved to be highly influenced by changes in the surface geometry and effective emissivity of the substrate. Therefore, absolute measurements of the surface temperature were not possible, but the pyrometer signal can give insight into the dynamics of the deposition process.

The photograph of Fig. 2 (right) shows the red laser processing head mounted under a window of the LA-MOCVD chamber via external *X-Y-Z* stages allowing for position and focus adjustments of the laser spot with respect to the sample mounted inside the chamber.

2.3 Sample characterization methods

For scanning electron micrographs (SEM) and energy dispersive X-ray spectra (EDX) of the samples, a scanning electron microscope Zeiss Supra 40 (Oberkochen, Germany), operated in InLens- and SE-mode at 10 kV electron acceleration voltage, was used. It was not necessary to additionally overcoat the sample surfaces for good conductivity.

The instrument used for Raman characterization was integrated in a *Laser Nanofactory* workstation of Femtika (Vilnius, Lithuania). It consisted of a 532 nm cw laser with 50 mW power and a 20×/0.8 microscope objective lens, producing a spot size of ~ 0.81 µm at the sample surface. A Kymera grating spectrograph (Oxford Instruments, Abingdon, UK) and a CCD camera from Andor Technology (Belfast, Northern Ireland) with 1600 × 200 pixels of 16 µm × 16 µm size, resulted in a spectral resolution of 0.05 to 0.07 nm for analyzing the back-scattered radiation of the Raman laser. The information depth of the probing Raman laser radiation crucially depends on the analyzed material and was estimated to be of the order of 0.1 µm for the CISe material here.

3 Thermo-physical simulation

To simulate the laser heating process and to determine the local temperature distribution on the surface of the molybdenum-covered glass substrate, a thermo-physical model was implemented: the heat conduction equation for a material system consisting of a molybdenum layer and a glass substrate was solved for steady-state conditions, i.e. for the absorbed cw laser irradiation as source term of the generated heat, within the given boundary conditions.

The heat conduction equation was numerically solved via finite-element-method-simulation (software FlexPDE version 6.37 from PDE Solutions Inc, Spokane, WA, USA) on a windows PC (Windows 10) with 4 GHz and 16 GHz memory. To speed-up the calculation using radial coordinates, the size of the glass substrate was limited to a radius of 2000 µm (30 times larger than typical spot sizes), and the laser beam was assumed to be concentric with a radially symmetric Gaussian profile in good agreement with the actual laser profile used. The reflection coefficient of the molybdenum surface for laser radiation of 1070 nm wavelength was taken to be 70% [16]. For the thermal conductivity of molybdenum and soda-lime glass constant values of 118 W/(m·K) (at 550 °C) [17] and 1.2 W/(m·K) [18] were used, respectively.

In the simulations, the backside of the glass substrate was held at a constant temperature of 380 °C. The sample was assumed to be thermally insulated and radiative heat transport was neglected here.

Convective heat loss from the temperature-controlled sample surface (typ. 380 °C) to the surrounding gas, which was pre-heated to 50 °C in the delivery tubes, was tested by introduction of a heat transfer coefficient in the model. Even at a high value of 50 W/(m^2·K), this coefficient had a negligible effect on the temperature rise in the laser-heated area but was mainly affecting the surface temperature of the whole substrate, thus an effect that was experimentally compensated for by the temperature controller. Therefore, convective heat losses were neglected in the simulation results presented here, leaving heat conduction in the molybdenum layer and glass substrate as the only heat transfer mechanisms.

4 Results and discussion

4.1 Thermo-physical simulations

The intensity profile of the incident radiation (reduced by the transfer losses of 7%) of a laser beam with a Gaussian profile of 61.5 µm radius is depicted in blue in Fig. 3 along with the resulting simulated temperature profile (red trace) at the surface of a 380 nm thick molybdenum layer on a 2 mm thick soda-lime-silicate glass substrate. The peak intensity for 255 mW power is 4.0 kW/cm^2, resulting in a peak temperature rise of 219 K for the Mo film above the nominal pre-heating temperature of the glass substrate.

The temperature distribution with a FWHM of 156 µm is approximately twice as wide as the laser irradiation spot with a FWHM of 80 µm, but falling-off with a broader decay towards the edges of the sample. It was verified that the temperature profiles scale linearly with respect to the incident laser power.

An exploration of the influence of the molybdenum layer thickness and Gaussian laser beam width on the temperature profile is presented in Fig. 4 for 113 mW laser power. Decreasing the laser beam radius by 30% from 61.5 µm (red trace) to 43.5 µm (green trace), while leaving the molybdenum layer thickness constant at 380 nm, increases the simulated peak surface temperature rise by 24% from 97 to 120 K. The corresponding width of the temperature profile decreases by 24% to FWHM of 120 µm resulting in a better confinement of heat in the irradiated spot.

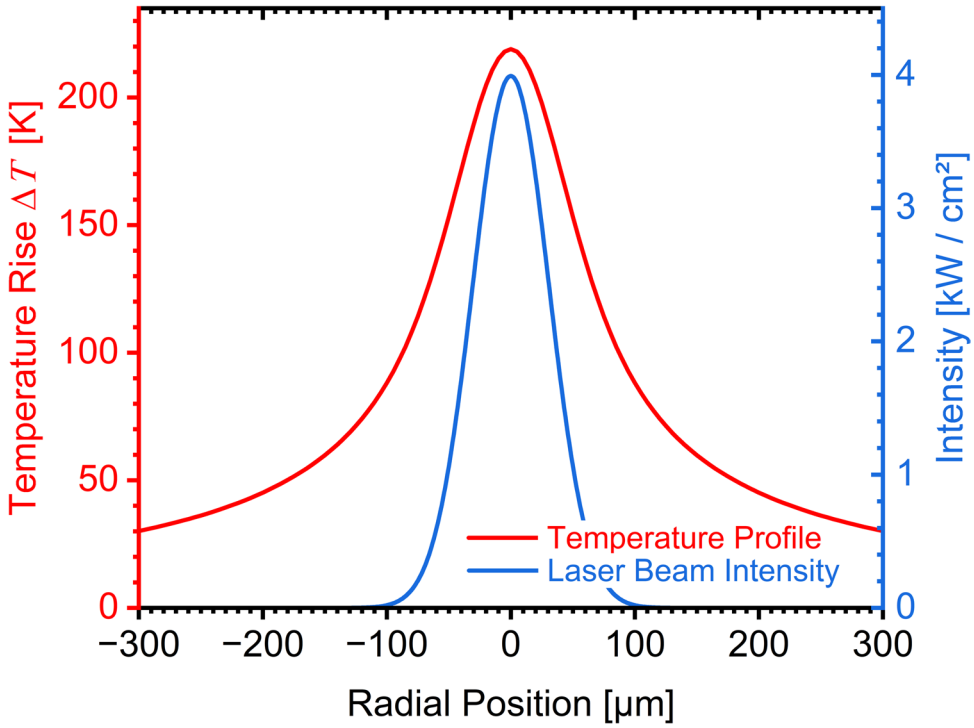

Fig. 3 Simulated surface temperature rise (red trace) above the heater temperature of 380 °C at the surface of a 2 mm thick glass substrate, coated with a 380 nm thick molybdenum layer upon local heating with laser radiation (blue trace) of 255 mW power with a Gaussian beam profile of 61.5 µm spot size radius

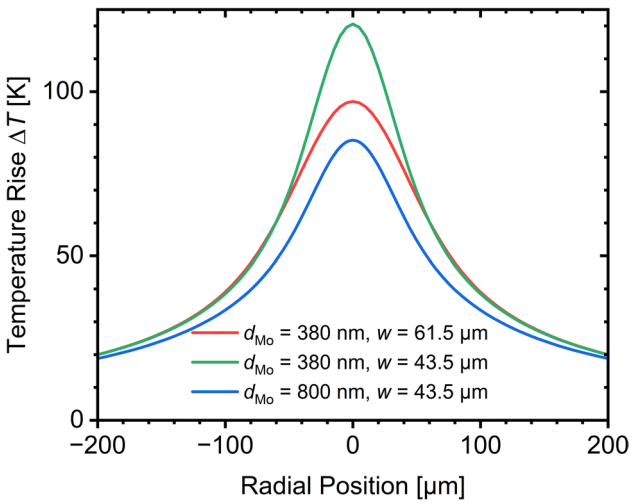

Fig. 4 Simulated surface temperature rise of a 2 mm thick glass substrate coated with either a 380 nm (red and green trace) or an 800 nm (blue trace) thick molybdenum layer and pre-heated to a nominal temperature of 380 °C. In addition, the substrate is locally heated with laser radiation of 113 mW power with a Gaussian beam profile spot size radius of 61.5 µm (red trace) or 43.5 µm (green and blue traces), respectively

On the other hand, a thicker molybdenum layer of 800 nm (blue trace) aids in the lateral heat transfer due to the about 100× better thermal conductivity of molybdenum compared to the glass substrate. The temperature profile becomes wider with a FWHM of 142 µm but with a reduced simulated peak surface temperature rise of 85 K for 113 mW laser power.

4.2 LA-MOCVD

The effect of irradiating the molybdenum layer in absence of gaseous trimethylindium was investigated for different laser powers to determine the possible process window. At elevated laser power levels, it appears that the laser radiation is causing a modification of the molybdenum visible as increased microroughness in SEM micrographs.

A local change in morphology caused by the laser radiation on the molybdenum film may facilitate the surface wetting by indium and consequently the formation of indium clusters, as observed in previous investigations [8].

However, an intact molybdenum layer is essential for further processing and the electrical contacts of micro solar cells. Experiments with high peak intensities exceeding 10.9 kW/cm^2 (resulting in a simulated peak temperature above 800 °C) led to cracks in a molybdenum layer of 275 nm thickness and additionally indicated the melting of the underlying soda-lime glass substrate by forming shallow surface depressions. This scenario is supported by EDX measurements (data not shown here) of the cracked region that showed peaks for Si and O_2, that were not visible on the molybdenum layer away from the laser irradiated spots or after irradiation with lower laser power.

For indium deposition, the substrates were pre-heated to a nominal temperature of 380 °C and held at this temperature for typically one hour with the flow of trimethylindium and carrier gas to ensure that a thermal equilibrium was reached. Subsequently, the laser was switched on. The

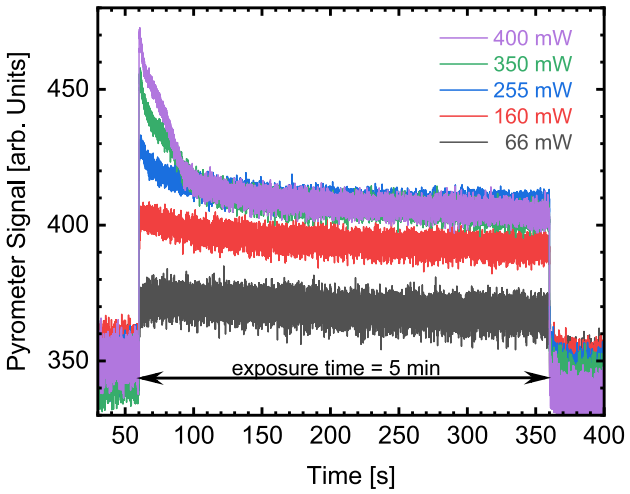

Fig. 5 Pyrometer signal (2000-2600 nm band) for five laser power levels of 66 mW (black trace), 160 mW (red trace), 255 mW (blue trace), 350 mW (green trace) and 400 mW (purple trace). SEM-micrographs of the resulting indium deposition spots are shown in Fig. 6

process diagrams of Fig. 5 depict examples of the temporal laser irradiation process and the resulting pyrometer signal for five different laser powers. The laser was turned on 60 s after start of the recording and then held at a constant power level during the sample exposure time of 5 min.

Prior to the indium deposition with formation of indium droplets and other modifications of the surface, the pyrometer signal is indicative of surface temperature. As seen in Fig. 5, the pyrometer signal increase is linear in laser power in the first seconds of irradiation. At later times, during indium deposition, the pyrometer signal is strongly affected by the surface condition (optical reflectivity, thermal emissivity, topography, etc.) and is not a reliable indicator of surface temperature. For times between 100 and 360 s, the effects of higher surface temperature and enhanced surface modification largely cancel each other to result in overlapping values of pyrometer signal. After cessation of the laser irradiation (times after 360 s) the surfaces processed at higher laser powers have smaller pyrometer signal values, although all samples should have returned to the starting temperature by this time.

The series of SEM micrographs of Fig. 6a-d displays the deposition of indium in the form of micrometric beads with increasing laser power from 160 to 400 mW. Experimental conditions were a 380 nm thick molybdenum layer, a Gaussian beam radius of (61.5 ± 7) µm, and 5 min exposure time. Underneath the light-colored indium beads, a dark area can be observed in the SEM micrographs, termed "black halo" throughout this publication; its diameter increases with laser power. Supposedly, it is associated with a slight variation in electrical surface conductivity and only visible in the surface sensitive InLens mode chosen here for

Fig. 6 SEM-micrographs of indium deposition on a molybdenum film due to local laser irradiation with increasing power and exposure of 5 min duration, taken in surface sensitive InLens imaging mode of the SEM. a) 160 mW, b) 255 mW, c) 350 mW, d) 400 mW

surface inspection. Under the optical microscope the black halo appears as a lighter colored surface area. Taking the thermo-physical simulation results into consideration, it can be concluded that the black halos are formed at substrate temperatures above ~ 460 °C. This might be attributed to the formation of an electrically conductive adhesion layer, which may contain metallic indium or carbon originating from trimethylindium.

The inner zone of the indium deposition spot, reaching higher temperatures due to the Gaussian laser spot profile (compare Fig. 3), exhibits a higher area density of indium beads in the center. Reaching a laser power of 255 mW or a peak intensity of 4.0 kW/cm^2 (Fig. 6b), the indium beads start to accumulate in the middle to form a larger island, which will grow further in diameter with increasing laser power (Fig. 6c). The indium beads get densely packed to form an island of 66 µm diameter above 400 mW irradiation (Fig. 6d). Here, the peak temperature rise as predicted by the thermo-physical simulation is ~ 340 K.

This behavior is also reflected in the signal recorded with the pyrometer (Fig. 5). At a laser power of 66 mW, (black trace), without deposition of indium, the pyrometer signal stays nearly constant during the entire exposure time. At larger laser powers resulting in thermal decomposition of trimethylindium precursor gas, the pyrometer signal declines quickly after the initial temperature rise, due to a change in emissivity and surface topography of the forming molten indium beads. The more indium is deposited, the steeper the decline. The pyrometric profiles suggest that the formation of the dense island at 400 mW (Fig. 5, purple trace) visible in the SEM-micrograph in Fig. 6d causes an additional decline in the pyrometer signal. The indium deposition appears to happen within the first 30 s of the laser irradiation. Therefore, further depositions were conducted with shorter exposure times of 60 s. The indium beads were localized within the laser heated area. The areas surrounding the laser irradiated spot showed only little indium deposition.

EDX spectra (Fig. 7) depict only the characteristic peaks of indium for the beads (blue trace). The red trace, taken on the substrate area in between the droplets within the black halo, has high peaks at the characteristic emission line of molybdenum at ~ 2.3 keV but also small peaks of indium at ~ 3.25 keV and ~ 3.5 keV. The green trace recorded outside of the black halo region without visible deposition of indium is almost identical to the red trace. This points to adsorption of indium or gaseous trimethylindium on the molybdenum surface.

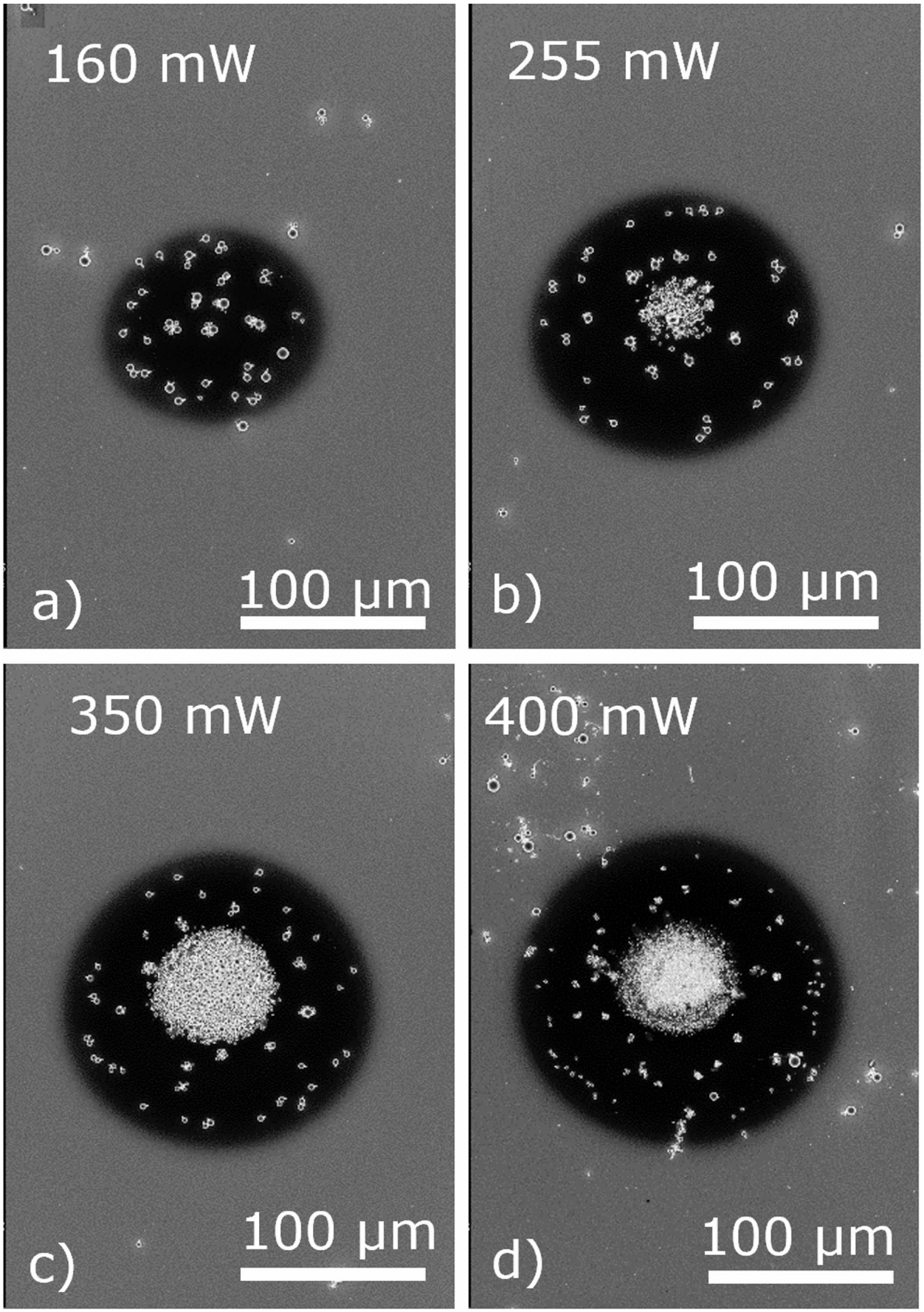
160 mW
a)
100 µm
255 mW
b)
100 µm
350 mW
c)
100 µm
400 mW
d)
100 µm

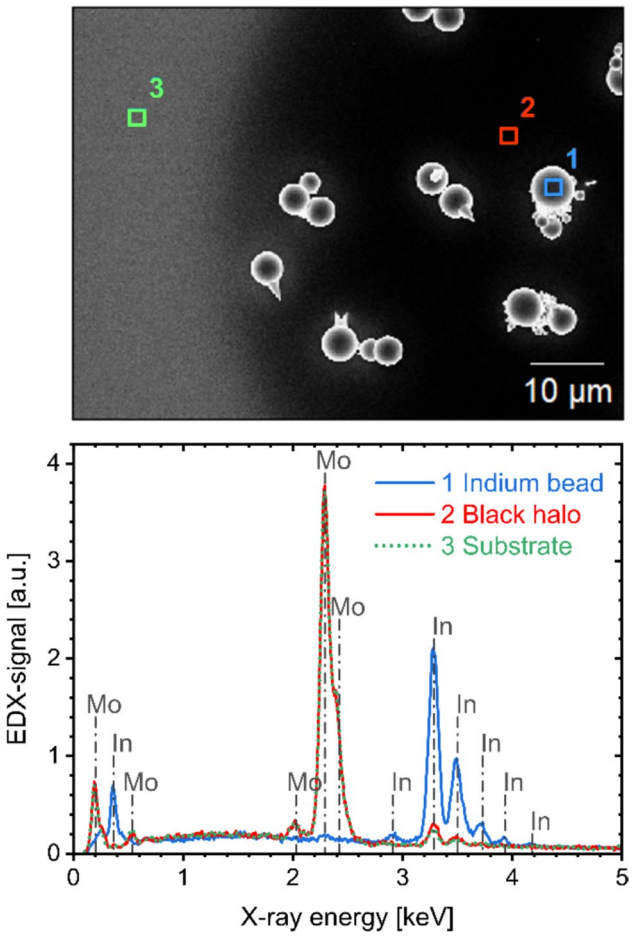

Fig. 7 SEM-micrograph of a detail of the deposition spot of Fig. 6a with a laser power of 160 mW and an exposure time of 5 min (upper panel). Corresponding EDX spectra (lower panel). The blue trace was recorded on an indium bead ((1) in the upper micrograph), the red trace in between the beads within the black halo (2), and the green trace on the unaffected substrate area (3)

In order to prepare micro solar cells, an effective electrical contact between the beads and the substrate is essential, and cracks in the molybdenum layer might lead to short circuits. Thicker molybdenum films would reduce the thermal load of the micro-concentrator solar cell due to better heat conduction. Moreover, the molybdenum back contact is more stable during the selenization step and be less likely to be fully converted to $MoSe_2$.

Increasing the molybdenum layer thickness to 800 nm while working with a tighter focused beam of (43.5 ± 5) µm confines the temperature rise to a smaller area, as seen in the thermo-physical simulation of Fig. 4, blue trace. The FWHM of the simulated temperature distribution is 140 µm. To reach a sufficient peak intensity of 3.5 kW/cm^2, the laser power can be reduced to 113 mW. The peak temperature rise is then only 85 K compared to 219 K in the previous configuration.

Figure 8a illustrates an indium precursor island grown using the above-mentioned parameters, with the nominal substrate temperature reduced to 350 °C and a shorter exposure time of 1 min. The figure reveals the growth of densely assembled small indium micro-beads, arranged into a larger island. The diameters of the beads are 1–3 µm in the center of the island and gradually decrease towards the edges to sub-micrometer dimensions. The island has a diameter of ~ 73 µm. There are very few beads outside the dense cluster due to the reduced substrate temperature.

This precursor island was processed into a $CuInSe_2$ absorber by depositing 800 nm of copper and subsequent annealing in selenium atmosphere at a maximum of 700 °C (for details see experimental section). During this process, the absorber increased in height from ~ 1 µm as In precursor island to 2.7 µm as CISe absorber island, while retaining its initial width. Additionally, the sample was etched with KCN to remove any excess $CuSe_x$ before capturing the SEM image shown in Fig. 8b. The fabricated absorber island exhibits a densely packed grain structure without pinholes. With increasing laser power, mainly the diameter of the solar absorber island changed.

As depicted in Fig. 8c, the sample was analyzed using micro-Raman spectroscopy, comparing the absorber island (blue curve) with a reference spot far from the island (red curve). On the island, the only visible sharp Raman peak at 175 cm^{-1} corresponds to the CISe absorber signal, indicating that the island is sufficiently dense to block the $MoSe_2$ signal. Moving away from the laser deposition spot to a reference position, a pronounced $MoSe_2$ peak appears at 245 cm^{-1}, while the absorber peak remains visible. This observation suggests that the entire sample is covered with a thin layer of absorber, which does not affect its usability for solar cell production. The broad band around 850 cm^{-1} arises from the glass material of the microscope objective used in the micro-Raman spectroscopic measurements and is not related to the sample.

For the joint assessment of the experimental data, it can be concluded that a laser power of 113 mW (incident peak intensity of 3.5 kW/cm^2), leading to a calculated temperature rise of 85 K, and exposure times of 1 min were sufficient to grow an indium precursor and to process it into a CIGSe solar absorber island. In view of the initially determined process window for the laser power and surface temperatures, this leaves a fivefold process margin between the temperature rise of 85 K needed for deposition of indium and the 420 K temperature rise with respect to the preheated substrate temperature of 380 °C, leading to laser-induced damage of the molybdenum coated glass substrate.

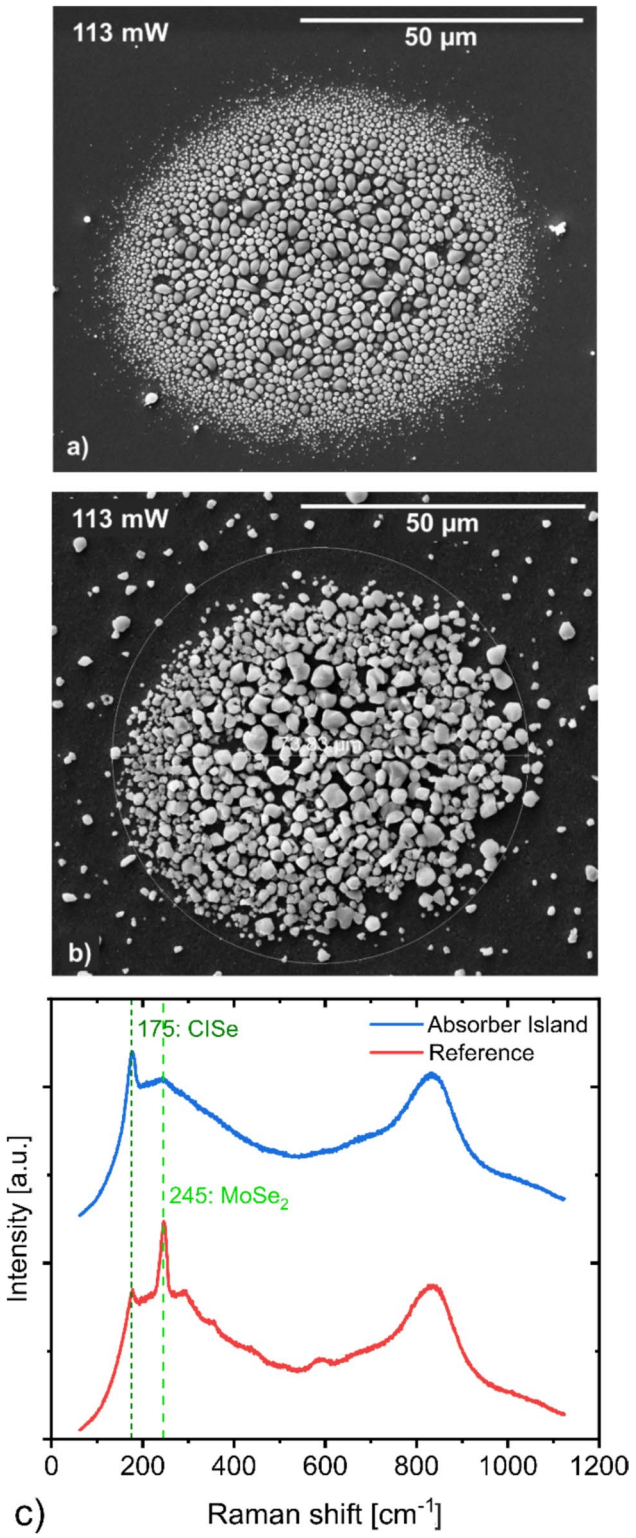

Fig. 8 SEM-micrographs of a) Indium precursor and b) $CuInSe_2$ solar absorber island. Process parameters for precursor growth: 1 min laser irradiation with 113 mW power, 1000 sccm nitrogen flow, 100 sccm trimethylindium flow and 350 °C nominal substrate temperature. For absorber growth: 800 nm of deposited copper and selenization at 700°C. c) Raman spectra taken on the absorber island (blue curve) and at a reference spot far away from the island (red curve)

5 Conclusion

Spatially selective deposition of indium on molybdenum films due to laser heating with a low-cost continuous-wave infrared laser was successfully demonstrated. Exposure times of 1 min and laser peak intensities of 3.5 kW/cm^2 were sufficient to decompose gaseous trimethylindium and deposit indium in a localized island consisting of tightly packed micro-beads. These indium aggregations were further processed to CISe absorber islands for potential use in applications like micro-concentrator solar cells. The feature size can be modified by the spot size and power of the laser beam and the thickness of the molybdenum layer used. It is possible to scale up the process for the simultaneous production of precursors by using several laser beams in parallel.

Acknowledgements Parts of this work were performed at the electron microscopy center at BAM. The authors would like to thank T. Lange (BAM 6.1) for the SEM and EDX characterizations, M. Weise (BAM 6.1) for tactile profilometry, and S. Cinque (BAM 6.2) for the support with the laser setup.
The Raman measurements were performed on a Next-Gen Cluster-Tool funded by the Deutsche Forschungsgemeinschaft (DFG, German Research Foundation)—INST 20876/347-1 FUGG and are acknowledged as follows: "Gefördert durch die Deutsche Forschungsgemeinschaft (DFG)—Projektnummer INST 20876/347-1 FUGG".

Authors' contributions Conceptualization: Heike Voss, Jörn Bonse, Torsten Boeck, Jens Martin, Martina Schmid, Jörg Krüger; Methodology, Data curation, Formal analysis and investigation: Heike Voss, Setareh Zahedi-Azad, Jan Lucaßen, Guido Mann; Writing—original draft preparation: Heike Voss; Writing – Jörn Bonse, Jörg Krüger; Review and editing: Heike Voss, Setareh Zahedi-Azad, Owen Ernst, Jan Lucaßen, Guido Mann, Jörn Bonse, Torsten Boeck, Jens Martin, Martina Schmid, Jörg Krüger; Funding acquisition: Torsten Boeck, Martina Schmid, Jörg Krüger; Project administration: Torsten Boeck, Jens Martin, Martina Schmid, Jörg Krüger.

Funding Open Access funding enabled and organized by Projekt DEAL. This research was funded by the German Federal Ministry for Economic Affairs and Climate Action (BMWK) under the contract numbers 03EE1029A (IKZ), 03EE1029C (BAM), and 03EE1029D (UDE).

Data availability The data supporting the findings of the study are available from the corresponding author upon reasonable request.

Declarations The authors have no relevant financial or non-financial interests to disclose.

References

1. M. Schmid, Revisiting the definition of solar cell generations. Adv. Opt. Mater. **11**, 2300697 (2023). https://doi.org/10.1002/adom.202300697
2. M. Alves, A. Pérez-Rodríguez, P.J. Dale, C. Domínguez, S. Sadewasser, Thin-film micro-concentrator solar cells. J. Phys. Energy **2**, 012001 (2020). https://doi.org/10.1088/2515-7655/ab4289
3. M. Alves, P. Anacleto, V. Teixeira, J. Carneiro, S. Sadewasser, Fabrication of pre-structured substrates and growth of CIGS micro-absorbers. Nanomaterials **14**, 543 (2024). https://doi.org/10.3390/nano14060543
4. M. Paire, L. Lombez, N. Péré-Laperne, S. Collin, J.-L. Pelouard, D. Lincot, J.-F. Guillemoles, Microscale solar cells for high concentration on polycrystalline Cu(In,Ga)Se_2 thin films. Appl. Phys. Lett. **98**, 264102 (2011). https://doi.org/10.1063/1.3604789
5. M. Paire, A. Shams, L. Lombez, N. Péré-Laperne, S. Collin, J.-L. Pelouard, J.-F. Guillemoles, D. Lincot, Resistive and thermal scale effects for Cu(In, Ga)Se_2 polycrystalline thin film microcells under concentration. Energy Environ. Sci. **4**, 4972 (2011). https://doi.org/10.1039/C1EE01661J
6. A. Duchatelet, K. Nguyen, P.-P. Grand, D. Lincot, M. Paire, Self-aligned growth of thin film Cu(In,Ga)S_e2 solar cells on various micropatterns. Appl. Phys. Lett. **109**, 253901 (2016). https://doi.org/10.1063/1.4971975
7. D. Siopa, K. El Hajraoui, S. Tombolato, F. Babbe, A. Lomuscio, M.H. Wolter, P. Anacleto, K. Abderrafi, F.L. Deepak, S. Sadewasser, P.J. Dale, Micro-sized thin-film solar cells via area-selective electrochemical deposition for concentrator photovoltaics application. Sci. Rep. **10**, 14763 (2020). https://doi.org/10.1038/s41598-020-71717-0
8. F. Ringleb, K. Eylers, T. Teubner, T. Boeck, C. Symietz, J. Bonse, S. Andree, J. Krüger, B. Heidmann, M. Schmid, M. Lux-Steiner, Regularly arranged indium islands on glass/molybdenum substrates upon femtosecond laser and physical vapor deposition processing. Appl. Phys. Lett. **108**, 111904 (2016). https://doi.org/10.1063/1.4943794
9. B. Heidmann, F. Ringleb, K. Eylers, S. Levcenco, J. Bonse, S. Andree, J. Krüger, T. Unold, T. Boeck, M.C. Lux-Steiner, M. Schmid, Local growth of $CuInSe_2$ micro solar cells for concentrator application. Mater. Today Energy **6**, 238–247 (2017). https://doi.org/10.1016/j.mtener.2017.10.010
10. S. Andree, B. Heidmann, F. Ringleb, K. Eylers, J. Bonse, T. Boeck, M. Schmid, J. Krüger, Production of precursors for micro-concentrator solar cells by femtosecond laser-induced forward transfer. Appl. Phys. A **123**, 670 (2017). https://doi.org/10.1007/s00339-017-1282-x
11. B. Heidmann, S. Andree, S. Levcenko, T. Unold, D. Abou-Ras, N. Schäfer, J. Bonse, J. Krüger, M. Schmid, Fabrication of regularly arranged chalcopyrite micro solar cells via femtosecond laser-induced forward transfer for concentrator application. ACS Appl. Energy Mater. **1**, 27–31 (2018). https://doi.org/10.1021/acsaem.7b00028
12. F. Ringleb, S. Andree, B. Heidmann, J. Bonse, K. Eylers, O. Ernst, T. Boeck, M. Schmid, J. Krüger, Femtosecond laser-assisted fabrication of chalcopyrite micro-concentrator photovoltaics. Beilstein J. Nanotechnol. **9**, 3025–3038 (2018). https://doi.org/10.3762/bjnano.9.281
13. T.F. Deutsch, D.J. Ehrlich, R.M. Osgood Jr., Z.L. Liau, Ohmic contact formation on InP by pulsed laser photochemical doping. Appl. Phys. Lett. **36**, 847–849 (1980). https://doi.org/10.1063/1.91345
14. M. Trippel, J. Bläsing, M. Wieneke, A. Dadgar, G. Schmidt, F. Bertram, J. Christen, A. Strittmatter, Laser-assisted local metal–organic vapor phase epitaxy. Rev. Sci. Instrum. **93**, 113904 (2022). https://doi.org/10.1063/5.0092251
15. C.A. Larsen, G.B. Stringfellow, Decomposition kinetics of OMVPE precursors. J. Cryst. Growth **75**, 247–254 (1986). https://doi.org/10.1016/0022-0248(86)90034-5
16. M.M. Kirillova, L.V. Nomerovannaya, M.M. Noskov, Optical properties of molybdenum single crystals. Sov. Phys. JETP **33**, 1210–1214 (1971) http://www.jetp.ras.ru/cgi-bin/dn/e_033_06_1210.pdf
17. Netzsch, 2025 Website NETZSCH-Gerätebau GmbH: https://analyzing-testing.netzsch.com/en/application-literature/measurement-of-the-thermophysical-properties-of-pure-molybdenum Accessed on May 11, 2025.
18. H. Kiyohashi, N. Hayakawa, S. Aratani, H. Masuda, Thermal conductivity of heat-absorbed soda-lime-silicate glasses at high temperatures. High Temp. - High Pressures **34**, 167–176 (2002).